



## 1 Analysis of the MODIS Above-Cloud Aerosol Retrieval

## 2 Algorithm Using MCARS

3

4 Galina Wind<sup>1,2</sup>, Arlindo M. da Silva<sup>2</sup>, Kerry G. Meyer<sup>2</sup>, Steven Platnick<sup>2</sup> and Peter  
5 M. Norris<sup>3,2</sup>

6 [1] SSAI, Inc. 10210 Greenbelt Road, Suite 600, Lanham, Maryland 20706, USA

7 [2] NASA Goddard Space Flight Center, 8800 Greenbelt Rd. Greenbelt, Maryland, 20771,  
8 USA

9 [3] Universities Space Research Association, 7178 Columbia Gateway Dr., Columbia, MD  
10 21046, USA

11 Correspondence to: G. Wind (Gala.Wind@nasa.gov)

12



### 13 Abstract

14 The Multi-sensor Cloud and Aerosol Retrieval Simulator (MCARS) presently produces  
15 synthetic radiance data from Goddard Earth Observing System version 5 (GEOS-5) model  
16 output as if the Moderate Resolution Imaging Spectroradiometer (MODIS) was viewing a  
17 combination of atmospheric column inclusive of clouds, aerosols and a variety of gases and  
18 land/ocean surface at a specific location. In this paper we use MCARS to study the MODIS  
19 Above-Cloud AEROSol retrieval algorithm (MOD06ACAERO). MOD06ACAERO is  
20 presently a regional research algorithm able to retrieve aerosol optical thickness over clouds,  
21 in particular absorbing biomass burning aerosols overlying marine boundary layer clouds in  
22 the Southeastern Atlantic Ocean. The algorithm's ability to provide aerosol information in  
23 cloudy conditions makes it a valuable source of information for modeling and climate studies  
24 in an area where current clear sky-only operational MODIS aerosol retrievals effectively have  
25 a data gap between the months of June and October. We use MCARS for a verification and  
26 closure study of the MOD06ACAERO algorithm.

27 Our simulations indicate that the MOD06ACAERO algorithm performs well for marine  
28 boundary layer clouds in the SE Atlantic provided some specific screening rules are observed.  
29 For the present study, a combination of five simulated MODIS data granules was used for a  
30 dataset of 13.5 million samples with known input conditions. When pixel retrieval uncertainty  
31 was less than 30%, optical thickness of the underlying cloud layer was greater than 4 and  
32 scattering angle range within the cloud bow was excluded, MOD06ACAERO retrievals  
33 agreed with the underlying ground truth (GEOS-5 cloud and aerosol profiles used to generate  
34 the synthetic radiances) with a slope of 0.913, offset of 0.06, and RMSE=0.107. When only  
35 near-nadir pixels were considered (view zenith angle within +/-20 degrees) the agreement  
36 with source data further improved (0.977, 0.051 and 0.096 respectively). Algorithm closure  
37 was examined using a single case out of the five used for verification. For closure, the



38MOD06ACAERO code was modified to use GEOS-5 temperature and moisture profiles as  
39ancillary. Agreement of MOD06ACAERO retrievals with source data for the closure study  
40had a slope of 0.996 with offset -0.007 and RMSE of 0.097 at pixel uncertainty level of less  
41than 40%, illustrating the benefits of high-quality ancillary atmospheric data for such  
42retrievals.



## 431 Introduction

44

45 The MODerate resolution Imaging Spectroradiometer (MODIS) (Barnes et al., 1998) has  
46 proven to be an important sensor for aerosol data assimilation purposes for models such as the  
47 Goddard Earth Observing System Model, Version 5 (GEOS-5; Rienecker et al. 2008, Molod  
48 et al. 2012). There are two MODIS instruments on board NASA’s Earth Observing System  
49 (EOS) *Terra* and *Aqua* spacecraft. There is a wide variety of data products available from  
50 these instruments for Land, Ocean and Atmosphere disciplines. Atmosphere discipline  
51 products include cloud mask, cloud top properties, cloud optical and microphysical properties  
52 and atmospheric aerosol properties. The MODIS data product files use a designation of MOD  
53 for Terra MODIS and MYD for Aqua MODIS. In this paper for brevity we will use “MOD”  
54 to refer to both instruments.

55 The largest contributor of biomass burning aerosols is Southern Africa (Reid et al, 2009,  
56 van der Werf et al, 2010). Biomass burning occurring from June through October creates thick  
57 smoke plumes that extend over the adjacent Atlantic Ocean. Prevailing winds in the area  
58 transport the smoke over the Southeast Atlantic Ocean (SEAO) and then as far as the  
59 Americas (Swap et al., 1996). The same time period coincides with a near-persistent layer of  
60 marine boundary-layer (MBL) stratus cloud that extends for several hundred miles westward  
61 from the Namibian coast (Devasthale and Thomas, 2011). The MODIS Dark Target aerosol  
62 retrieval algorithm (MOD04) that is used for ocean retrievals operates in clear sky conditions  
63 only. MOD04\_DT retrievals are not provided for each individual MODIS pixel-level, but  
64 rather are performed over a 3x3 or 10x10 set of pixels. Moreover aerosol properties are not  
65 retrieved over sun glint regions (Kaufman et al, 1997, Levy et al, 2009, 2013). The SEAO  
66 region has both extensive seasonal cloud cover and a significant portion of MODIS granules



67containing sun glint, leading to equally extensive loss of continuous observations from the  
68area.

69 Figure 1 illustrates these conditions using Terra MODIS data from 2006 through 2013.  
70Panel a) shows the percentage of ocean gridboxes in the SEAO area that had daily mean cloud  
71fraction greater than 50% in the MODIS Daily Level-3 gridded product (add reference) stored  
72at 1x1 degree resolution. Here, the SEAO area is defined the same way as in Meyer et al  
73(2015), specifically between -20 and +20 degrees longitude and +4 to -20 degrees longitude.  
74As much as 60% of all ocean gridboxes have cloud fraction greater than 50% in June (day  
75152) and only increase to the end of September (day 304). A 1-degree resolution gridbox will  
76contain some clear sky and thus at least some aerosol retrievals are possible. As shown in  
77Figure 1 b), in June about 70% of all ocean gridboxes contain some aerosol retrievals, though  
78by September that number drops to about 30-40%.

79 Due to aforementioned limitations of the standard dark-target MODIS aerosol algorithm,  
80a model that assimilates aerosol data from SEAO would have very few aerosol retrievals over  
81the ocean available to it. Most of the transport mechanism in the model would be thus  
82governed by the model physical processes (e.g., advection, sedimentation and wet removal  
83and vertical transport) instead of being constrained by observations.

84 The MOD06ACAERO algorithm (Meyer et al. 2015) fills in the aerosol data gap in  
85SEAO as it is able to perform retrievals of aerosol properties above MBL clouds. The  
86algorithm has been evaluated against observations from the Cloud-Aerosol Lidar and Infrared  
87Pathfinder Satellite Observation (CALIPSO) (Winker et al, 2009), but CALIPSO only  
88provides data at nadir and with a very limited spatial coverage. Recent improvements in  
89CALIPSO version 4 aerosol products (Kim et al, 2018) indicate that the comparisons shown  
90of the MOD06ACAERO algorithm with CALIPSO in Meyer et al (2015) would improve



91 somewhat as significant work had been done to remedy the low bias that CALIPSO retrievals  
92 have. However, Kim et al (2018) state that the remaining SEA low bias in CALIPSO  
93 retrievals of AOD with respect to AERONET and MODIS makes CALIPSO retrievals  
94 somewhat problematic as means of aerosol algorithm evaluation for SEAO area. (e.g., Meyer  
95 et al, 2013, 2015, Jethva et al, 2014). Observations collected during the Observations of  
96 Aerosols above Clouds and their Interactions (ORACLES) (Redemann et al, 2019) are  
97 currently being used to evaluate the MOD06ACAERO algorithm.

98 In this study we applied an Observing System Simulation Experiment (OSSE) framework  
99 to gain insight on the performance of the MOD06ACAERO algorithm. Rather than using the  
100 classic analysis/forecast error metric common in Numerical Weather Prediction OSSE studies  
101 (e.g., Hoffman and Atlas 2016) we adopt here a “Retrieval OSSE” perspective where the  
102 quality of the retrieval is used as the verification metric (Wind et al. 2013, 2016). A radiative  
103 transfer code is applied to the model quantities combined with sensor geometry to simulate  
104 how a model scene appears to a specific instrument. A retrieval algorithm designed for that  
105 instrument can be executed on the simulated measurements. Physical quantities retrieved by  
106 the algorithm can be compared to the known simulation input. The algorithm can be examined  
107 for closure over a large spatial domain and thus any areas or conditions that may be  
108 problematic for the algorithm could be examined, and the strengths and limitations of the  
109 algorithm can be extensively documented.

110 The Multi-sensor Cloud and Aerosol Retrieval Simulator (MCARS) is a tool that  
111 combines model output with a radiative transfer code in order to simulate radiances that may  
112 be measured by a remote sensing instrument if it were passing over the model fields (Wind et  
113 al, 2013, 2016). In this paper, MCARS continues to use the combination of the GEOS-5  
114 model, correlated- $k$  models of atmospheric transmittance due to various gaseous absorbers for



115MODIS channels as per Kratz (1995), inline Rayleigh scattering and the Discrete Ordinate  
116Radiative Transfer (DISORT) code (Stamnes et al. 1988) to simulate MODIS radiances. Two  
117improvements have been made to the MCARS code since last publication. The computational  
118resolution has been increased to 32 streams, up from 16. Additionally, for this study the  
119higher resolution 7 km GEOS-5 Nature Run (G5NR) was used in place of the standard 25 km  
120resolution GEOS-5 output (Gelaro et al. 2015, da Silva et al. 2015, Putman et al. 2015).  
121G5NR is a 2-year global, non-hydrostatic mesoscale model dataset for the period 2005-2006  
122produced with the GEOS-5 Atmospheric GCM. The model run is performed at a horizontal  
123resolution of 7 km using a cubed-sphere horizontal grid with 72 vertical levels, extending up  
124to 0.01 hPa (~ 80 km). In addition to standard meteorological parameters (wind, temperature,  
125moisture, surface pressure), this GCM includes 15 aerosol tracers (dust, sea-salt, sulfate, black  
126and organic carbon), O<sub>3</sub> and CO<sub>2</sub>. The GEOS-5 NR is driven by prescribed sea-surface  
127temperature and sea-ice, daily volcanic and biomass burning emissions, as well as high-  
128resolution inventories of anthropogenic sources. A description of the GEOS-5 model  
129configuration used for the Nature Run can be found in Putman et al. (2014), while results  
130from a validation exercise appear in Gelaro et al. (2015) and Castellanos et al. (2019).

131 In a previous study of the MOD04\_DT code (Wind et al, 2016), we had the advantage of  
132having simultaneous in situ aerosol property measurements from AERosol RObotic NETwork  
133(AERONET) (Holben et al., 1998). AERONET has very limited data available over ocean,  
134mainly from islands and ship transits. Even in places where AERONET is established, no  
135measurements can be obtained in presence of clouds. Therefore, no ground-based in-situ  
136measurements can be included in our analysis of the MOD06ACAERO product and so the  
137analysis is necessarily limited to verification and closure.



138 In sections that follow we will describe the application of MCARS to study the  
139MOD06ACAERO algorithm. Section 2 very briefly describes the MCARS code and the  
140experiment setup. Section 3 describes the MODIS MOD06ACAERO product of Meyer et al.  
141(2015). Section 4 shows the details of the study and study conclusions. Finally, section 5  
142discusses the next steps in MCARS development.

### 1432 **MCARS description**

144 The MCARS code was previously described in detail in Wind et al (2013, 2016).  
145Therefore, only a brief description will be given here. Global aerosol, cloud, surface and  
146atmospheric column fields from the G5NR simulation as described above serve as the starting  
147point for radiance simulations. The GOCART bulk aerosol scheme currently used in the  
148G5NR is used for the simulations reported in this paper, with corresponding optical properties  
149as described in Randles et al. (2017), Hess et al (1998) and references within. The simulation  
150input data was produced in accordance with the methods outlined in Wind et al. (2016). The  
151G5NR model output was split into 1-km subcolumns (MODIS pixel resolution) using the  
152independent column approximation method as described in detail in Wind et al. (2013). Here  
153a brief summary of the model data preparation methodology is given.

154 MODIS pixels for each GEOS-5 gridbox were collected and the same number of pixel-  
155like sub-columns was generated using a statistical model of sub-gridcolumn moisture  
156variability. The sub-column generation used a parameterized probability density function  
157(PDF) of total water content for each model layer and a Gaussian copula to correlate these  
158PDFs in the vertical (Norris et al, 2008, Norris and da Silva 2016a,b).

159 The subcolumns generated in this way were subsequently rearranged, to give horizontal  
160spatial coherence, by using a horizontal Gaussian copula applied to condensed water path.  
161This arrangement had to be applied in order to create spatially coherent cloud-like structures.





162The subcolumns themselves were not altered in any way during this process. If this step is  
163skipped and the subcolumns are placed randomly within each gridbox the MODIS Cloud  
164Optical and Microphysical Properties (MOD06) product (Platnick et al, 2017) would restore  
165many of the pixels to clear sky unless the initial gridbox had close to 100% cloud fraction  
166(Zhang and Platnick 2011; Pincus et al. 2012). The MOD06 product is a necessary input for  
167MOD06ACAERO and must be produced prior to MOD06ACAERO execution. The need for  
168this subcolumn rearrangement is significantly lessened when G5NR is used because the  
169smaller gridboxes are often close to 100% cloudy especially in MBL regimes, but removing  
170the method from the model preparation step was not practical due to its small impact on  
171execution time and possibility of introducing errors.

172 The layer aerosol properties were obtained using the independent column approximation  
173with the same PDF of total water content as used for clouds. A GEOS-5 aerosol species  
174output file was used in conjunction with aerosol optical properties as in Randles et al. (2017).  
175The aerosol phase functions for each of the 15 species output by GEOS-5 were produced and  
176combined on the fly to create a single bulk set of scattering properties and Legendre  
177coefficients. (Wind et al, 2016)

178 Model parameters such as profiles of temperature, pressure, ozone and water vapor  
179together with layer information about clouds and aerosols are combined with solar and view  
180geometry of the MODIS instrument. Surface information is also a combination of GEOS-5  
181information of surface temperature, snow and sea ice cover and MODIS-derived spectral  
182surface albedo (Moody et al. 2007, 2008). All of these parameters are transferred to the  
183DISORT-5 radiative transfer code and reflectances and radiances in 22 MODIS channels  
184between 470nm and 14.2 $\mu$ m are produced. The default computational resolution of DISORT-  
185has also been increased to 32 streams up from 16 used in the two previous studies.  
186Additionally some of the simulations in this study were executed at 64 streams. Final MCARS



187output is packaged in a format identical to the standard MODIS Level-1B radiometric files  
188and is thus completely transparent to any operational or research-level retrieval algorithm  
189code.

190 These simulations were produced at the NASA Center for Climate Simulations (NCCS)  
191supercomputer. Each complete simulation of a MODIS-like granule requires 5.5 hours of wall  
192clock time on 300 processors. Computational throughput can be increased by limiting the  
193scope of the simulation to fit a particular investigation. For this study, however, we retain the  
194full set of channels needed for both cloud and aerosol research.

195

### 1963 **MODIS above-cloud aerosol properties product**

197

198 The MODIS above-cloud aerosol properties product (MOD06ACAERO) (Meyer et al.  
1992015) is a regional algorithm able to simultaneously retrieve MBL cloud optical thickness  
200(COT), cloud effective radius, and aerosol optical depth (AOD) above-cloud in the SEAO  
201region. It uses six MODIS channels (bands 1-5 and 7) having central wavelengths of 0.47,  
2020.55, 0.66, 0.86, 1.24 and 2.1 $\mu\text{m}$ . The MOD06ACAERO algorithm takes advantage of the  
203strong biomass burning aerosol absorption gradient in the visible (VIS) to near-infrared (NIR)  
204spectrum that, when the aerosol layer overlies a bright cloud, yields differential attenuation  
205(stronger at shorter wavelengths) of the otherwise nearly spectrally invariant top-of-  
206atmosphere cloud reflectance across the VIS/NIR. Sensitivity to cloud optical thickness is  
207localized in the spectral range between 0.47 and 1.24 $\mu\text{m}$  and is directly related to the  
208magnitude of reflectance, while sensitivity to above-cloud aerosol optical depth is related to  
209the spectral slope of the reflectance. The MOD06ACAERO algorithm uses 2.1 $\mu\text{m}$  channel for  
210cloud effective radius information. That is also consistent with the principal retrieval  
211contained in the MOD06 product (Platnick, et al, 2017)



212 The MOD06ACAERO retrieval inversion uses an optimal estimation-like approach  
213 (Rodgers, 1976) that attempts to minimize the difference (cost function) between the six  
214 MODIS reflectance observations and forward-modeled reflectance that is a function of cloud  
215 optical thickness, effective radius, and above-cloud AOD. However, rather than in-line  
216 radiative transfer calculations, MOD06ACAERO relies on a set of pre-computed lookup  
217 tables (LUTs) of coupled cloud and above-cloud aerosol reflectance. These LUTs are  
218 generated using the same cloud microphysics models used by MOD06 (Platnick et al, 2017)  
219 and the absorbing aerosol model used by MOD04\_DT over land surfaces (Levy et al, 2013).  
220 Retrievals using a second aerosol property model, one based on field campaign data from  
221 SAFARI 2000 (Haywood et al, 2003), are also available in MOD06ACAERO output. While  
222 these Haywood et al. model retrievals were recommended in Meyer et al (2015), evaluation  
223 during the ORACLES campaign revealed deficiencies at certain scattering angle ranges (K.  
224 Meyer, private communication). Thus, for this study we use the MOD06ACAERO results  
225 based on the MOD04\_DT aerosol models.

226 The MOD06ACAERO retrieval operates at 1km resolution, compared to the 10km and  
227 3km MOD04\_DT resolutions, and simultaneously provides pixel-level estimates of retrieval  
228 uncertainty accounting for known and quantifiable error sources (e.g., radiometry,  
229 atmospheric profile errors, cloud and aerosol forward model errors) consistent with the  
230 MOD06 cloud product methodology (Platnick et al, 2020). Figure 2 shows an example  
231 retrieval result from MOD06ACAERO compared to MOD04\_DT standard 10km output. The  
232 Terra MODIS granule shown here, from 2006 day 224 at 10:05 UTC, has extensive cloud  
233 cover over the ocean, typical for this season. MOD04\_DT provides a very limited amount of  
234 data, localized to the few areas of clear sky, while MOD06ACAERO fills in the above-cloud  
235 area.

236 MOD06ACAERO uses National Center for Environmental Prediction (NCEP)



237atmospheric profile products (Derber et al, 1991) for atmospheric correction. As part of our  
238investigation we will look at impact of discrepancies between NCEP and G5NR on retrieved  
239aerosol properties.

240

#### 2414 **Analysis**

242

243 To create the data used for the MOD06ACAERO verification study, we examined the  
244G5NR dataset for cases that were similar to conditions commonly encountered during the  
245burning season over SEAO. August 2006 was selected because it was a very active smoke  
246season and a significant amount of MBL clouds were present in the model output. Models  
247often have difficulties forming MBL clouds as higher than usual grid and vertical resolution is  
248needed in order to accurately represent the processes that lead to MBL formation in nature.

249 As real Terra and Aqua overpasses are needed in order to define the sun-satellite  
250geometry for the MCARS simulations, satellite orbital tracks had to be considered. Because  
251orbital gaps are prominent in the MODIS data over the SEAO MBL region, care must be  
252taken in selecting specific days and times having adequate sensor geometry. Technically  
253because MCARS is a simulation, orbital gaps have no meaning. But because of the need of  
254actual sensor geometry to start the simulation, it is most expedient to simply browse available  
255MODIS data for a suitable track. Even though G5NR does not perform any data assimilation,  
256the model code is identical to the standard GEOS-5 model. MCARS normally runs on  
257standard GEOS-5 output. In Wind et al (2013) we showed MCARS as a model output  
258verification tool. It is always very desirable to match date/time/orbit when model performance  
259may be compared to real concurrent sensor measurements. Even though no orbital match is  
260required in this study, a decision was made to not alter the standard MCARS operation in  
261order to avoid accidental introduction of software issues. Five cases were selected under these



262 considerations. Three came from Terra MODIS overpasses and two from Aqua MODIS. The  
263 times and dates were as follows. Terra MODIS: 2006 day 224, 10:05 UTC, 2006 day 225  
264 09:10 UTC, 2006 day 228 09:40 UTC. Aqua MODIS: 2006 day 224 12:55 UTC and 2006 day  
265 226 12:40 UTC. This dataset comprises 13.5 million points where the atmospheric column  
266 and surface conditions are explicitly known.

267 Figure 3 a) shows simulated RGB images for the 5 MCARS MODIS granules listed  
268 above. Also shown in b) are the same simulated granules where the aerosols have been  
269 removed from the radiative transfer simulations. This ability to remove clouds, aerosols or  
270 gases from the simulation offers extensive control evaluating the performance of  
271 retrieval algorithms and diagnosing algorithm deficiencies.

272 There is a significant similarity between the real Terra MODIS granule of Figure 2 and  
273 the simulated granule for the same date and time. The G5NR is a free running model and does  
274 not perform any data assimilation, and therefore it is not synoptically locked to the particular  
275 day depicted in Figure 2. The apparent similarities between Figures 2 and 3 merely reflect the  
276 persistent patterns of MBL clouds and smoke in the region. There is no expectation of a match  
277 with any real data in this study. It is not a statement to G5NR performance as in other cases  
278 the cloud amount/distribution had no match to any real data. It is merely an interesting  
279 coincidence. Some granules were selected to include a significant portion of land surface for a  
280 later examination of the MOD04\_DT retrievals, repeating the study in Wind et al (2016) in a  
281 different region (not reported here).

282 This dataset, both the complete and the clean (aerosol-free) versions, was fed through the  
283 standard operational MODIS Data Collection 6 cloud product processing chain to produce  
284 cloud mask, MOD06 cloud top and optical properties, and finally the MOD06ACAERO  
285 output for each case. Results from all granules were then combined and only retrievals for  
286 cloudy pixels were examined. The MOD06ACAERO aerosol retrievals were compared to



287source aerosol optical depth provided by GEOS-5 (Wind et al, 2013). Figure 4 shows results  
288of this comparison. The only constraint on this comparison was that the algorithm-reported  
289pixel-level retrieval uncertainty had to be less than 40% for panel a) and less than 30% for  
290panel b). One of the motivations of this study was to characterize errors in the  
291MOD06ACAERO algorithm for subsequent aerosol data assimilation into GEOS-5. Pixels  
292with higher uncertainties could be considered in the analysis, but assimilating data where the  
293retrieval error is 50% or greater could negatively impact the assimilated fields. As depicted in  
294Figure 4, filtering retrievals at the reported algorithm uncertainty at 40% is very effective to  
295produce a good match between MOD06ACAERO and the G5NR output variables, with the  
296exception of very low AODs. G5NR uses aerosol models described in detail in Randles et al  
297(2017). It is a set of 15 absorbers, properties of which are a function of column relative  
298humidity. MOD06ACAERO in this study uses the MOD04\_DT aerosol models, which are  
299distinct in composition and additionally computed at a constant 80% column relative humidity  
300(Levy et al, 2013). Because G5NR mixes aerosols on-the-fly to create bulk layer properties  
301and MOD06ACAERO has a constant regional mixture, there is a natural source of uncertainty  
302in any comparison of MOD06ACAERO retrievals with G5NR. However the regional mixture  
303of MOD04\_DT had been used extensively to train the GOCART model used by both GEOS-5  
304and G5NR. Thus we expect the uncertainty due to aerosol model mismatch to be fairly  
305minimal. Same exact situation of aerosol mixture mismatch exists in real data and is most  
306likely greater than the one existing in this simulation.

307 Meyer et al. (2015) suggest that additionally MOD06ACAERO retrievals should be  
308screened by retrieved cloud optical thickness and that they should be discarded if COT is less  
309than 4.0. We applied this additional constraint onto the retrieval comparison and the result is  
310shown in Figure 5. Discarding the AOD retrievals when cloud is thin improved the match-up  
311against GEOS-5, but there still appears to be an issue when GEOS-5 AOD is very close to



312zero.

313 The power of MCARS lies in being able to tightly control simulation parameters. The  
314MOD06ACAERO algorithm appears to run into a difficulty at low source AOD. In order to  
315examine the causes for this discrepancy in more detail, we turn our attention to the clean  
316MCARS case shown in figure 3b) by setting the AOD precisely to zero and examining the  
317retrieval performance in such situation. Ideally MOD06ACAERO should retrieve a zero AOD  
318throughout. With an exception of a narrow range of scattering angles between 135 and 145  
319degrees, which corresponds to the cloud bow direction, the algorithm indeed retrieved AOD  
320that was extremely close to zero. Figure 6 depicts the difference between retrieval and source  
321as a function of scattering angle. Retrievals where MOD06ACAERO matched GEOS-5  
322precisely were discarded for clarity. Within the cloud bow MOD06ACAERO tends to return a  
323small positive AOD of about 0.15.

324 The liquid water phase function is very complex in the cloudbow region and is very  
325difficult to model accurately. That particular region has consistently caused difficulties to the  
326standard MOD06 product retrievals of MBL clouds. Both MOD06 and MOD06ACAERO  
327LUTs are computed at 64 DISORT streams. We performed some investigation of this area by  
328running a special simulation for a single case from Terra 2006 day 224 10:05 UTC. This case  
329was selected because the cloudbow is especially noticeable in both real and simulated data.  
330The simulation was also executed using 64 DISORT streams in order to reduce uncertainties  
331associated with the simulation being performed at half the resolution. In cloudbow region  
332more streams would potentially lead to a better model. Unfortunately the cloudbow persisted.  
333It thus may be the case that 64 streams are not sufficient to properly resolve the cloudbow in  
334either simulation or retrieval. Even higher resolution may be advisable. Increasing  
335computational resolution of MOD06 LUTs is presently considered for the upcoming MODIS  
336Data Collection 7. Depending on the results, same increase may occur for MOD06ACAERO.



337At this time, for purpose of establishment of assimilation constraints, which is the focus of  
338this study, one might simply exclude the cloud bow scattering angle range from consideration  
339until more is known.

340 Figure 7 shows the results of MOD06ACAERO retrievals from Figure 5 where retrievals  
341within the cloud bow have been discarded. The comparison with source data is further  
342improved and the cluster of MOD06ACAERO retrievals present in Figure 5 when GEOS-5  
343AOD was near zero has disappeared.

344 Often better retrievals can be obtained when less oblique view geometry is considered in  
345real data. Pixel size, longer optical path length and 3D effects from clouds can all make  
346retrievals performed at oblique view angles less optimal. In the case of this study, another  
347consideration for imposition of a view zenith limit is that presently MCARS does not account  
348for pixel size growth at oblique view angles. The number of subcolumns generated does not  
349change with view zenith angle. Therefore, MCARS results when view angle is oblique may  
350not be an accurate measure of algorithm performance as only the effects of optical path length  
351are simulated.

352 The MOD06 cloud product outputs cloud top pressure, temperature and height limited to  
353near nadir in addition to full swath products. The “near nadir” is defined as viewing zenith  
354angle less than 32 degrees (Menzel et al, 2008). Figure 8 shows the MOD06ACAERO  
355retrievals of Figure 7 further limited by view zenith angle of less than 32 degrees. When view  
356zenith angle is limited to 32 degrees the comparison with GEOS-5 source data is again  
357improved. We can now show a slope of 0.866 for retrievals with less than 40% error and  
3580.913 for retrievals with error of less than 30%. Note that even though the data extent had  
359been limited, there are still over 600,000 data points left to be ingested into a model if data  
360assimilation were to be attempted in an area where previously the number of such data points  
361was close to 0.





362 We can constrain the view zenith angle range even further as shown in Figure 9, reducing  
363 the threshold to 20 degrees. Whereas the comparison shows all around improvement with  
364 slope of 0.931 and 0.977 for retrieval error of less than 40% and 30% respectively, the number  
365 of points suitable for assimilation shrinks by half. It is not clear if this dataset size reduction  
366 can be justified by the improvement in alignment with the source data.

367 With the 20 degree view angle constraint the algorithm results are very close to source  
368 data and we could potentially state that we have closure against source GEOS-5 data even  
369 though both MOD06 and MOD06ACAERO run under operational conditions used NCEP  
370 GDAS data for atmospheric correction (implying a likely overestimation of the error in these  
371 profiles). In order to assess the impact of using these GDAS-based profiles we consider a final  
372 experiment where we use MCARS pixel-level input profiles for atmospheric correction. The  
373 result is shown in Figure 10. When atmospheric profiles are removed as a source of  
374 inconsistency, the agreement with source data improves to a slope of 0.996 with intercept of -  
375 0.007 and RMSE of 0.097 for retrievals with less than 40% error and slope of 0.989, intercept  
376 of 0.03 and RMSE of 0.085 for retrievals with less than 30% error. Small sample size for  
377 retrievals with lower uncertainty is the reason for somewhat lesser agreement with source data  
378 for this closure experiment. The remaining source of potential disagreement of  
379 MOD06ACAERO retrieval with input GEOS-5 data is the difference between aerosol models  
380 used by MCARS and MOD06ACAERO. Cloud models between MOD06ACAERO and  
381 MCARS are identical in this study. The MOD06ACAERO model is fixed for the region,  
382 while the GEOS-5 aerosols are fully dynamic as per Randles et al (2017). However, it is not  
383 practical to change either MCARS or MOD06ACAERO code to use a different aerosol model  
384 set, and with the agreement being as good as it presently is.

385



## 3865 **Conclusions and future directions**

387 This paper is a direct evolution of work started in Wind et al, (2013) and continued in  
388 Wind et al (2016). The Multi-sensor Cloud and Aerosol Retrieval Simulator (MCARS) has  
389 now been applied as a verification tool for a research-level algorithm. The algorithm studied  
390 was the MODIS above-cloud aerosol properties retrieval algorithm of Meyer et al (2015).  
391 MCARS computational resolution has been doubled and for this study the high-resolution  
392 (7km) GEOS-5 Nature Run model was utilized. The MCARS code produces radiances and  
393 reflectances in a standard MODIS Level 1B format after sending the GEOS-5 data through  
394 DISORT-5 radiative transfer code. The output can be directly ingested by any retrieval or  
395 analysis code that reads data from the MODIS instrument.

396 We used the MCARS code to perform verification and closure study on the  
397 MOD06ACAERO algorithm. In this study we generated a set of five MODIS granules located  
398 in the Southeastern Atlantic Ocean off the coast of Namibia. We executed the  
399 MOD06ACAERO code on this case set. In the verification part of the study the algorithm  
400 performed very well. When pixels with less than 30% uncertainty were considered with  
401 underlying cloud layer having optical thickness greater than 4 the algorithm matched the  
402 source GEOS-5 aerosol optical depth with slope of 0.774 and offset of 0.076, RMSE = 0.131.  
403 On further examination, executing the algorithm on the same case set with aerosols removed it  
404 was determined that there might be data that is less useful around the scattering angle of 140  
405 degrees, the cloud bow direction. When the cloud bow pixels were excluded the slope  
406 improved to 0.913. The near-nadir slope with angle limit of 20 degrees improved the  
407 agreement further to 0.977, RMSE=0.096.

408 To look at closure one of the five cases was selected. For closure both MOD06 and  
409 MOD06ACAERO codes were modified to use MCARS input profiles as ancillary instead of  
410 the NCEP analysis used in operations (Platnick et al, 2017). When the results were compared



411 to source GEOS-5 data a slope of 0.996 with offset of -0.007 and RMSE = 0.097 was reached  
412 for pixels with less than 40% uncertainty. The agreement was slightly worse for uncertainties  
413 less than 30% (slope 0.989, offset 0.03 and RMSE = 0.085) but that was mainly due to having  
414 a smaller number of pixels in the set, only 130,000.

415 The results of this study suggest that retrievals produced by MOD06ACAERO are of  
416 good initial quality and would be a valuable addition to model data assimilation streams with  
417 the following constraints. MOD06ACAERO pixels should be assimilated if retrieval  
418 uncertainty is less than 40%, if optical thickness of the underlying cloud layer is greater than  
419 4.0 and if the pixel scattering angle is outside the cloud bow. Additionally, an even tighter  
420 constraint can be added to only take pixels that are near nadir.

421 This study is yet another example of the capabilities of the MCARS framework. There  
422 are many other potential applications of the MCARS code, including extending the simulator  
423 to other sensors and examining the performance of fast retrieval simulators used in climate  
424 modeling.

#### 4256 Code and Data Availability

426 The MCARS code and any datasets produced, including all data shown (GEOS-5 input  
427 in netCDF4 and all MODIS output in HDF4 file format) and discussed in this paper, are  
428 available to users free of charge by contacting the authors. There may be additional, wider  
429 distribution means in the future as needed. We have not deemed it practical up to this time to  
430 release the MCARS source code into general-purpose source repositories. The data files are  
431 quite large with source input data being on the order of 20 Gb for each MODIS-like granule  
432 created. The GEOS-5 model source code is publicly available, and we may release the  
433 MCARS code under the same NASA Open Source Agreement and the same repository.  
434



#### 435 **Author Contributions**

436 GW is the development and experiment design lead on the MCARS project. She  
437 maintains the code, creates experiments and performs most of the analysis of experiment data.

438 AdS and PN assist with preparation, interpretation and integration of the GEOS-5 model  
439 data.

440 KM is the author of MODIS above-cloud aerosol retrieval algorithm, the subject of this  
441 simulation experiment. He assisted with interpretation of retrieval results and development of  
442 assimilation constraints for the above-cloud aerosol product.

443 SP assisted with analysis, evaluation and interpretation of all experiment data.

444

#### 445 **Acknowledgements**

446 The authors would like to thank Brad Wind for the initial idea for creating a simulator,  
447 the output of which could be transparently used with remote sensing retrieval codes.

448

449



## 451     **References**

- 452 Barnes, W. L., T. S. Pagano, and V. V. Salomonson, 1998: Prelaunch characteristics of the  
453 Moderate Resolution Imaging Spectroradiometer (MODIS) on EOS-AM1. *IEEE Trans.*  
454 *Geosci. Remote Sens.*, 36, 088–1100.
- 455 Castellanos, P., da Silva, A., Darnenov, A., Buchard, V., Govindaraju, R., Ciren, P., &  
456 Kondragunta, S. (2019). A Geostationary Instrument Simulator for Aerosol Observing  
457 System Simulation Experiments. *Atmosphere*, 10(1), 2–36.  
458 <http://doi.org/10.3390/atmos10010002>
- 459 Chin, M., P. Ginoux, S. Kinne, O. Torres, B. N. Holben, B. N. Duncan, R. V. Martin, J. A.  
460 Logan, A. Higurashi, and T. Nakajima, 2002: Tropospheric Aerosol Optical Thickness  
461 from the GOCART Model and Comparisons with Satellite and Sun Photometer  
462 Measurements. *J. Atmos. Sci.*, 59, 461–483.  
463
- 464 da Silva, A.M., W. Putman and J. Nattala, 2014: File Specification for the 7-km GEOS-5  
465 Nature Run, Ganymed Release (Non-hydrostatic 7-km Global Mesoscale Simulation).  
466 GMAO Office Note No. 6 (Version 1.0), 176 pp, available from  
467 [http://gmao.gsfc.nasa.gov/pubs/office\\_notes](http://gmao.gsfc.nasa.gov/pubs/office_notes).  
468
- 469 Derber J.C., D.F. Parrish and S.J. Lord, 1991: The new global operational analysis system at  
470 the National Meteorological Center. *Weath. Forec.* 6, 538-547.
- 471 Devasthale, A., and M. A. Thomas 2011: A global survey of aerosol-liquid water cloud  
472 overlap based on four years of CALIPSO-CALIOP data. *Atmos. Chem. Phys.*, 11, 1143–  
473 1154, doi:10.5194/acp-11-1143-2011
- 474 Gelaro, R., W. Putman, S. Pawson, C. Draper, A. Molod, P.M. Norris, L.E. Ott, N. Prive, O.  
475 Reale, D. Achuthavarier, M. Bosilovich, V. Buchard, W. Chao, L. Coy, R. Cullather, A.M.  
476 da Silva, A. Darnenov, R.M. Errico, M. Fuentes, M.J. Kim, R. Koster, W. McCarty, J.  
477 Nattala, G. Partyka, S. Schubert, G. Vernieres, Y. Vikhliav, K. Wargan, 2015: Evaluation  
478 of the 7-km GEOS-5 Nature Run. Technical Report. NASA/TM-2014-104606, Goddard  
479 Space Flight Center, National Aeronautics and Space Administration.
- 480 Haywood, J. M., S. R. Osborne, P. N. Francis, A. Keil, P. Formenti, M. O. Andreae, and P. H.  
481 Kaye, 2003: The mean physical and optical properties of regional haze dominated by  
482 biomass burning aerosol measured from the C-130 aircraft during SAFARI 2000, J.  
483 *Geophys. Res.*, 108(D13), 8473, doi:10.1029/2002JD002226.
- 484 Hess, M., P. Koepke, and I. Schult, 1998: Optical properties of aerosols and clouds: The  
485 software package OPAC. *B. Am. Meteorol. Soc.*, 79(5), 831–844.
- 486 Hill, C., C. DeLuca, V. Balaji, M. Suarez, A. da Silva, 2004: The architecture of the Earth  
487 System Modeling Framework, *Comp. Sci. Engr.*, 6(1), 18-28.
- 488 Hoffman, R. N. and R. Atlas, 2016: Future Observing System Simulation Experiments.  
489 *BAMS*, 97(9), 1601–1616. <http://doi.org/10.1175/BAMS-D-15-00200.1>
- 490 Holben, B.N., T. F. Eck, I. Slutsker, D. Tanre, J.P. Buis, A. Setzer, E.F. Vermote, J. A.  
491 Reagan, Y.J. Kaufman, T. Nakajima, F. Lavenu, I. Jankowiak, A. Smirnov, 1998:  
492 AERONET – A federated instrument network and data archive for aerosol characterization.  
493 *Rem. Sens. Env.*, v.66, n1, p1-16.
- 494 Hsu, N.C., M-J. Jeong, C. Bettenhausen, A.M. Sayer, R. Hansell, C.S. Sefter, J. Huang, S-C.



- 495 Tsay 2013: Enhanced Deep Blue aerosol retrieval algorithm: The second generation. *J.*  
496 *Geophys. Res.-Atmos.*, 118(16), p 9296-9315.
- 497Hubanks, P., S. Platnick, M.D. King, W. Ridgway, 2019: MODIS Level-3 daily gridded  
498 product. <https://modis-atmos.gsfc.nasa.gov/images/l3-daily-browse>
- 499Jethva, H., O. Torres, F. Waquet, D. Chand, D., & Y. Hu, 2014: How do A-train sensors  
500 intercompare in the retrieval of above-cloud aerosol optical depth? A case study-based  
501 assessment. *Geophysical Research Letters*. [http://doi.org/10.1002/\(ISSN\)1944-8007](http://doi.org/10.1002/(ISSN)1944-8007)
- 502Kaufman, Y. J., A. E. Wald, L. A. Remer, B. C. Gao, R. R. Li, L. Flynn, 1997: The MODIS  
503 2.1 $\mu$ m channel - Correlation with visible reflectance for use in remote sensing of aerosol  
504 *IEEE Trans. Geosci. Remote Sens.*, Vol. 35, 1286-1298.
- 505Kim, M.-H., Omar, A. H., Tackett, J. L., Vaughan, M. A., Winker, D. M., Trepte, C. R., Hu,  
506 Y., Liu, Z., Poole, L. R., Pitts, M. C., Kar, J., and Magill, B. E.: The CALIPSO version 4  
507 automated aerosol classification and lidar ratio selection algorithm, *Atmos. Meas. Tech.*,  
508 11, 6107–6135, <https://doi.org/10.5194/amt-11-6107-2018>, 2018.
- 509Kratz, D.P. 1995: The correlated-k distribution technique as applied to the AVHRR channels.  
510 *J. Quant. Spectrosc. Rad. Trans.* 53, 501-517.
- 511Levy, R. C., S. Mattoo, L. A. Munchak, L. A. Remer, A. M. Sayer, F. Patadia, and N. C.  
512 Hsu, 2013: The Collection 6 MODIS aerosol products over land and ocean, *Atmos. Meas.*  
513 *Tech.*, 6, 2989-3034, doi:10.5194/amt-6-2989-2013.
- 514Levy, R.C., L. A. Remer, D. Tanre, S. Mattoo, Y.J. Kaufman, 2009: Algorithm for remote  
515 sensing of tropospheric aerosol over dark targets from MODIS Collections 005 and 051,  
516 revision 2. ATBD Reference Number: ATBD-MOD-04. [http://modis-](http://modis-atmos.gsfc.nasa.gov/reference_atbd.html)  
517 [atmos.gsfc.nasa.gov/reference\\_atbd.html](http://modis-atmos.gsfc.nasa.gov/reference_atbd.html)
- 518Menzel, W. P., R. Frey, H. Zhang, D. Wylie, C. Moeller, R. Holz, B. Maddux, B. A. Baum,  
519 K. Strabala, and L. Gumley, 2008: MODIS global cloud-top pressure and amount  
520 estimation: Algorithm description and results. *J. Appl. Meteor. Climatol.*, 47, 1175–1198.
- 521Meyer, K. G., S. Platnick. 2015: Simultaneously inferring above-cloud absorbing aerosol  
522 optical thickness and underlying liquid phase cloud optical and microphysical properties  
523 using MODIS. *J. Geophys. Res. Atmos.*, 120 (11): 5524–5547
- 524Meyer, K. G., S. Platnick, L. Oreopoulos, and D. Lee. 2013: Estimating the direct radiative  
525 effect of absorbing aerosols overlying marine boundary layer clouds in the southeast  
526 Atlantic using MODIS and CALIOP. *J. Geophys. Res. Atmos.*, 118 (10): 4801-4815
- 527Molod, A., L. Takacs, M. Suarez, J. Bacmeister, I.-S. Song, and A. Eichmann, 2012: The  
528 GEOS-5 Atmospheric General Circulation Model: Mean Climate and Development from  
529 MERRA to Fortuna. *Tech. Rep. S. Gl. Mod. Data Assim.*, 28
- 530Moody, E. G., M. D. King, C. B. Schaaf, D. K. Hall, and S. Platnick, 2007: Northern  
531 Hemisphere five-year average (2000-2004) spectral albedos of surfaces in the presence of  
532 snow: Statistics computed from Terra MODIS land products. *Remote Sens. Environ.*, 111,  
533 337–345.
- 534Moody, E. G., M. D. King, C. B. Schaaf and S. Platnick, 2008: MODIS-derived spatially  
535 complete surface albedo products: Spatial and temporal pixel distribution and zonal  
536 averages. *J. Appl. Meteor. Climatol.*, 47, 2879–2894.
- 537Norris, P. M., L. Oreopoulos, A. Y. Hou, W.-K. Tao, X. Zeng, 2008: Representation of 3D



538 heterogeneous cloud fields using copulas: Theory for water clouds. *J. Q. R. Meteorol. Soc.*  
539 134: 1843–1864. doi:10.1002/qj.321.

540Norris, P. M., and A. M. da Silva. 2016a: Monte Carlo Bayesian inference on a statistical  
541 model of sub-gridcolumn moisture variability using high-resolution cloud observations.  
542 Part 1: Method. *Q.J.R. Meteorol. Soc.*, 142 (699): 2505-2527.

543Norris, P. M., and A. M. da Silva. 2016b: Monte Carlo Bayesian inference on a statistical  
544 model of sub-gridcolumn moisture variability using high-resolution cloud observations.  
545 Part 2: Sensitivity tests and results. *Q.J.R. Meteorol. Soc.*, 142 (699): 2528-2540.

546Notarnicola, C., D. Di Rosa, F. Posa, 2011: Cross-Comparison of MODIS and CloudSat Data  
547 as a Tool to Validate Local Cloud Cover Masks. *Atmos.*, 2, 242-255,  
548 doi:10.3390/atmos2030242

549Pincus, R., S. Platnick, S. A. Ackerman, R. S. Hemler, and R. J. P. Hofmann, 2012:  
550 Reconciling simulated and observed views of clouds: MODIS, ISCCP, and the limits of  
551 instrument simulators. *J. Climate*, 25, 4699-4720. doi:10.1175/JCLI-D-11-00267.1.

552Platnick, S., K.G. Meyer, M.D. King, G. Wind, N. Amarasinghe, B. Marchant, G.T. Arnold, Z.  
553 Zhang, P.A. Hubanks, R.E. Holz, P. Yang, W. Ridgway and J. Riedi, 2017: The MODIS  
554 Cloud Optical and Microphysical Products: Collection 6 Updates and Examples from Terra  
555 and Aqua. *IEEE Trans. Geo. Rem. Sens.* 55(1), 502-525, doi:10.1109/TGRS.2016.2610522

556Platnick, S., K.G. Meyer, N. Amarasinghe, G. Wind, P.A. Hubanks and R.E. Holz 2020:  
557 Sensitivity of Multispectral Imager Liquid Water Cloud Microphysical Retrievals to the  
558 Index of Refraction. *Rem. Sens.* 2020, 12, 4165; doi:10.3390/rs12244165

559Putman W., A.M. da Silva, L.E. Ott and A. Darmanov, 2014: Model Configuration for the 7-  
560 km GEOS-5 Nature Run, Ganymed Release (Non-hydrostatic 7 km Global Mesoscale  
561 Simulation). GMAO Office Note No. 5 (Version 1.0), 18 pp, available from  
562 [http://gmao.gsfc.nasa.gov/pubs/office\\_notes](http://gmao.gsfc.nasa.gov/pubs/office_notes).

563Randles, C. A., A.M. da Silva, and V Buchar, 2017: The MERRA-2 Aerosol Reanalysis,  
564 1980–onward, Part I: System Description and Data Assimilation Evaluation. *Journal of*  
565 *Climate*. <http://doi.org/10.1175/JCLI-D-16-0609.s1>

566Redemann, J., R. Wood, B. Luna, K. Shiffer, 2019: ORACLES (ObseRvations of Aerosols  
567 above CLouds and their intEractionS) A NASA Earth Venture Suborbital Mission.

568 [https://espo.nasa.gov/oracles/content/ORACLES\\_Two-page\\_ORACLES\\_Flyer\\_LAD:](https://espo.nasa.gov/oracles/content/ORACLES_Two-page_ORACLES_Flyer_LAD_01.12.2021)  
569 [01.12.2021](https://espo.nasa.gov/oracles/content/ORACLES_Two-page_ORACLES_Flyer_LAD_01.12.2021)

570Reid, J. S., et al., 2009: Global monitoring and forecasting of biomass-burning smoke:  
571 Description of and lessons from the Fire Locating and Modeling of Burning Emissions  
572 (FLAMBE) program, *IEEE J. Sel. Top. Appl. Earth Obs. Remote Sens.*, 2, 144–162,  
573 doi:10.1109/JSTARS.2009.2027443.

574Rienecker, M.M., M. J. Suarez, R. Todling, J. Bacmeister, L. Takacs, H.-C. Liu, W. Gu, M.  
575 Sienkiewicz, R. D. Koster, R. Gelaro, I. Stajner, and J. E. Nielsen, 2008: The GEOS-5 Data  
576 Assimilation System - Documentation of Versions 5.0.1, 5.1.0, and 5.2.0. *Tech. Rep. S. Gl.*  
577 *Mod. Data Assim.*, 27

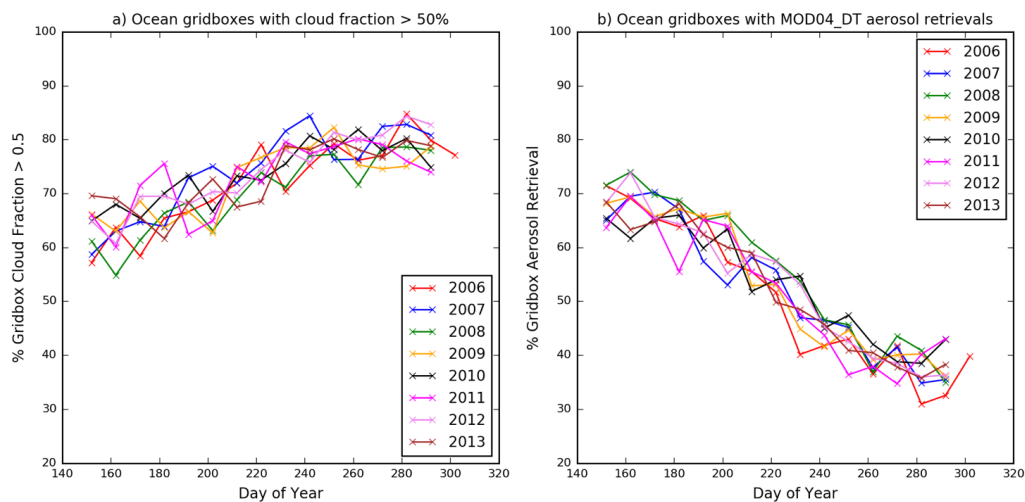
578Rodgers, C. D. (1976), Retrieval of atmospheric temperature and composition from remote  
579 measurements of thermal radiation, *Rev. Geophys. Space Phys.*, 14, 609–624.

580Swap, R., M. Garstang, S. A. Macko, P. D. Tyson, W. Maenhaut, P. Artaxo, P. Kallberg, and  
581 R. Talbot (1996), The long-range transport of southern African aerosols to the tropical



- 582 South Atlantic, *J. Geophys. Res.*, 101, 23,777–23,791, doi:10.1029/95JD01049.
- 583 van der Werf, G. R., et al., 2010: Global fire emissions and the contribution of deforestation,  
584 savanna, forest, agriculture, and peat fires (1997–2009), *Atmos. Chem. Phys.*, 10, 11,707–  
585 11,735, doi:10.5194/acp-10-11707-2010.
- 586 Wind, G., A.M. da Silva, P. M. Norris, and S. Platnick, 2013: Multi-sensor cloud retrieval  
587 simulator and remote sensing from model parameters – Part 1: Synthetic sensor radiance  
588 formulation, *Geosci. Model Dev.*, 6, 2049-2062, doi:10.5194/gmd-6-2049-2013.
- 589 Wind, G., A.M. da Silva, P.M. Norris, S. Platnick, S. Mattoo and R. C. Levy, 2016: Multi-  
590 sensor cloud retrieval simulator and remote sensing from model parameters – Part 2:  
591 Aerosols, *Geosci. Model Dev.*, 9, 2377-2389, doi:10.5194/gmd-9-2377-2016.
- 592 Zhang, Z., and S. Platnick, 2011: An assessment of differences between cloud effective  
593 particle radius for marine water clouds from three MODIS spectral bands. *J. Geophys.*  
594 *Res.*, 116, D20215, doi:10.1029/2011JD016216.
- 595

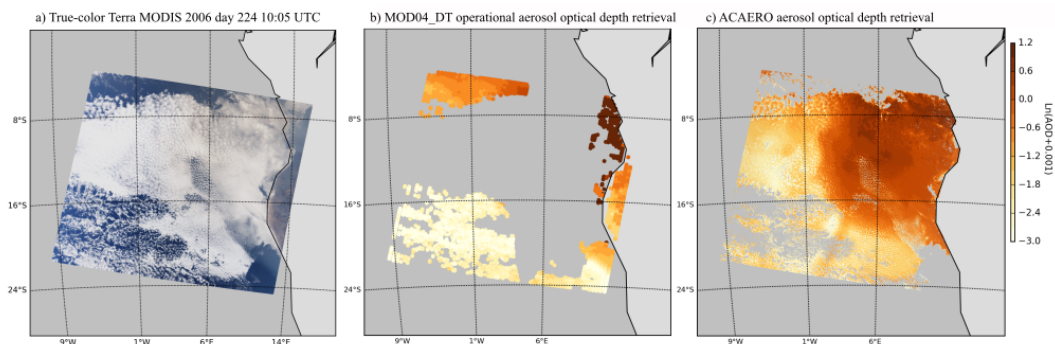




596  
597 Figure 1. Terra MODIS Level-3 Daily 1-degree gridded product for SEAO area for years  
598 2006-2013. Panel a) shows the percentage of SEAO ocean gridboxes that had cloud fraction  
599 greater than 50%. Panel b) shows the percentage of SEAO ocean gridboxes that had any  
600 successful MOD04DT aerosol property retrievals of any quality.  
601



602  
603



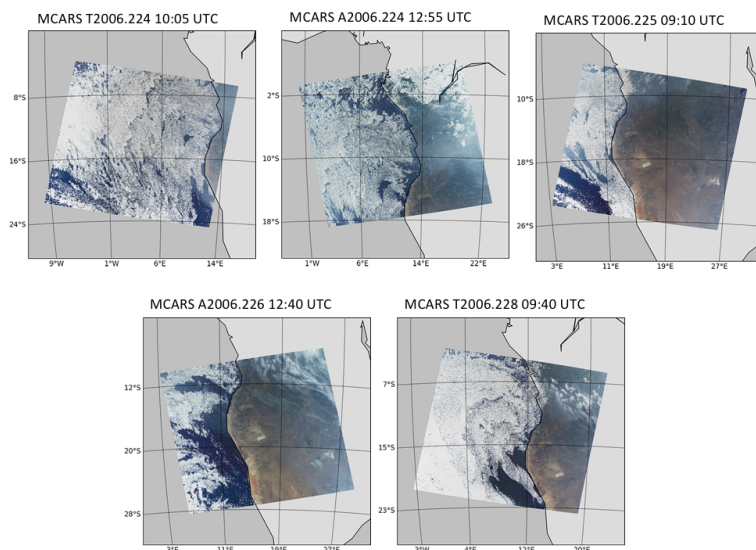
604  
605

606 Figure 2. Real-data example of MOD06ACAERO retrieval. Terra MODIS 2006 day 224  
607 10:05 UTC. Panel a) shows the true-color MODIS granule. There is extensive aerosol layer  
608 above the equally extensive MBL cloud layer. Panel b) shows the MODIS Data Collection 6  
609 operational Dark Target aerosol retrieval. It is a 10km resolution product with retrievals  
610 available only in clear sky conditions and outside glint. Panel c) shows the MOD06ACAERO  
611 above-cloud aerosol retrieval that is able to fill the data gap created by presence of MBL  
612 layer.

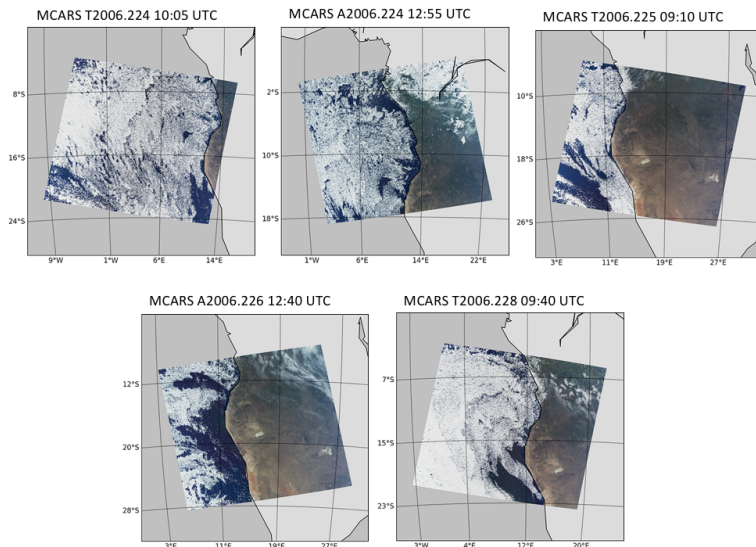
613  
614



a) MCARS study cases with aerosols included



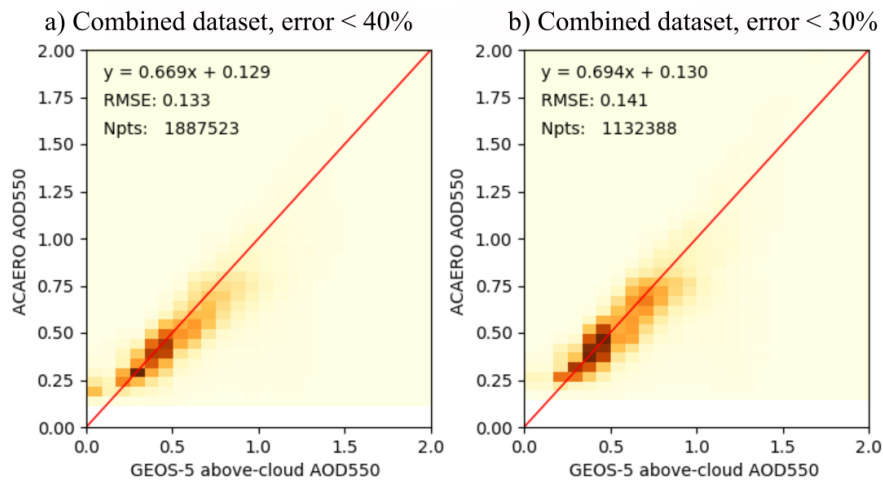
b) MCARS study cases with aerosols removed



615

616 Figure 3. Scenes generated by MCARS from G5NR used in analysis of the MOD06ACAERO  
617 product. There are three cases based on Terra MODIS, designated with a T next to the year.  
618 There are two cases based on Aqua MODIS, designated with an A next to the year. Panel a)  
619 shows the case set simulated with aerosols present. Panel b) shows the same case set but  
620 simulated with aerosols removed.

621

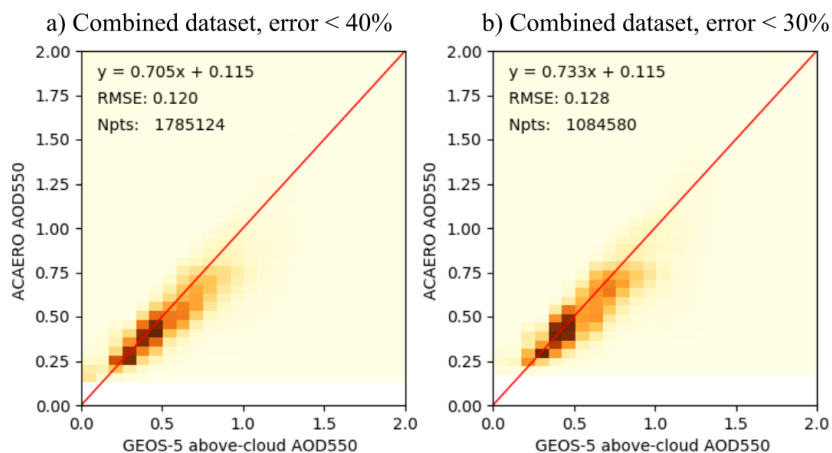


622

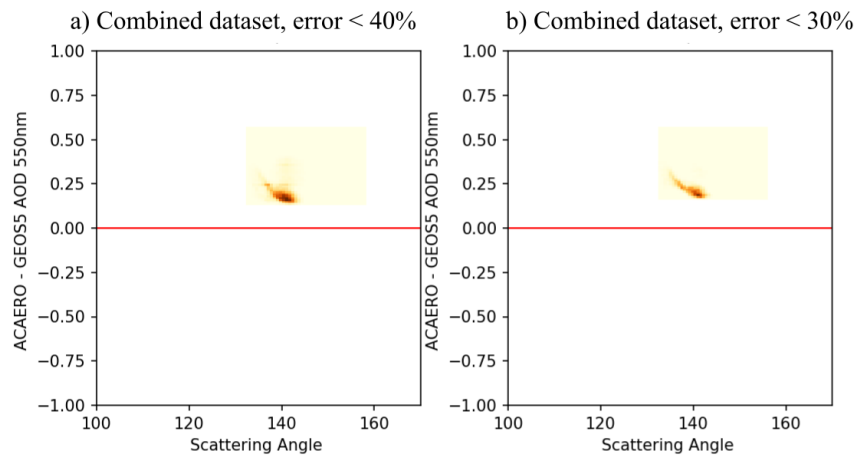
623 Figure 4. MOD06ACAERO retrieval results from the combined dataset of Figure 3a  
624 compared to source GEOS-5 aerosol optical depth. No screening of retrievals had been  
625 performed except for pixel-level uncertainty. Panel a) shows MOD06ACAERO retrievals  
626 with uncertainty of less than 40% and panel b) shows same with uncertainty less than 30%.

627

628

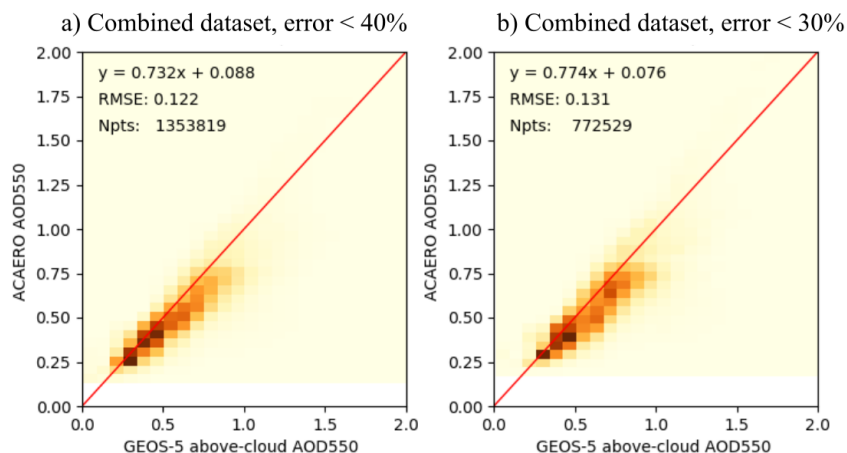


629 Figure 5. MOD06ACAERO retrieval results from the combined dataset of Figure 3a  
630 compared to source GEOS-5 aerosol optical depth. AOD retrievals where COT was less than  
631 4 are now discarded. Panel a) shows MOD06ACAERO retrievals with uncertainty of less than  
632 40% and panel b) shows same with uncertainty less than 30%.  
633



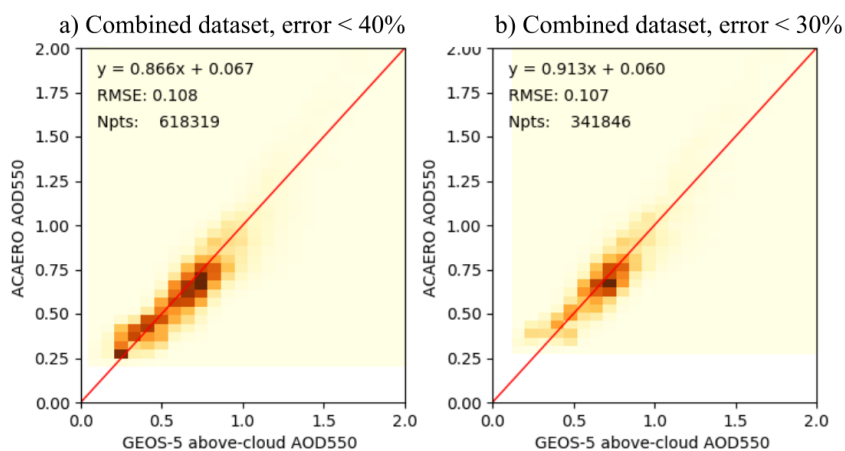
634 Figure 6. MOD06ACAERO retrieval results from the combined dataset of Figure 3b, where  
635 aerosols had been removed. The results are displayed as difference from GEOS-5 AOD,  
636 which in this case was zero, as a function of scattering angle. All retrievals where  
637 MOD06ACAERO result was also zero had been removed for clarity. All non-zero  
638 MOD06ACAERO retrievals appear to be concentrated in a narrow angle range between 135  
639 and 145 degrees which corresponds to the cloud bow. Panel a) shows MOD06ACAERO  
640 retrievals with uncertainty of less than 40% and panel b) shows same with uncertainty less  
641 than 30%.

642  
643



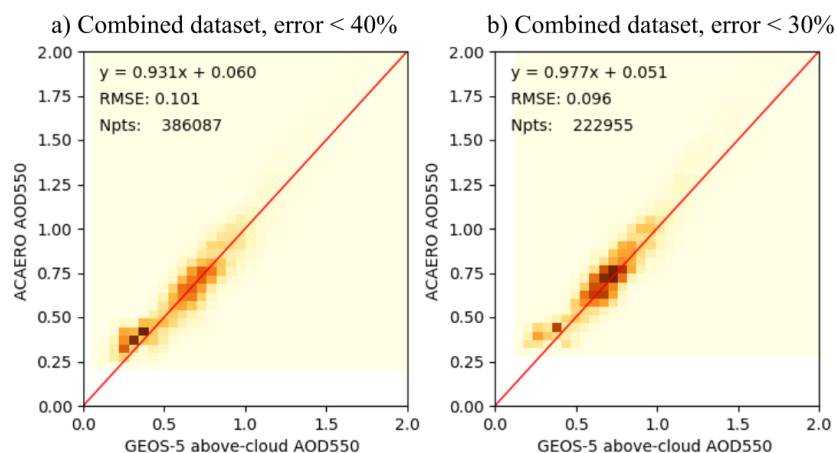
644 Figure 7. MOD06ACAERO retrieval results from the combined dataset of Figure 3a  
645 compared to source GEOS-5 aerosol optical depth. AOD retrievals where COT was less than  
646 are now discarded. Additionally retrievals in the cloud bow region are also removed. It  
647 appears they were indeed the source of a cluster of higher MOD06ACAERO retrievals when  
648 GEOS-5 AOD was near zero and the match up with GEOS-5 source AOD is further  
649 improved. Panel a) shows MOD06ACAERO retrievals with uncertainty of less than 40% and  
650 panel b) shows same with uncertainty less than 30%.

651  
652



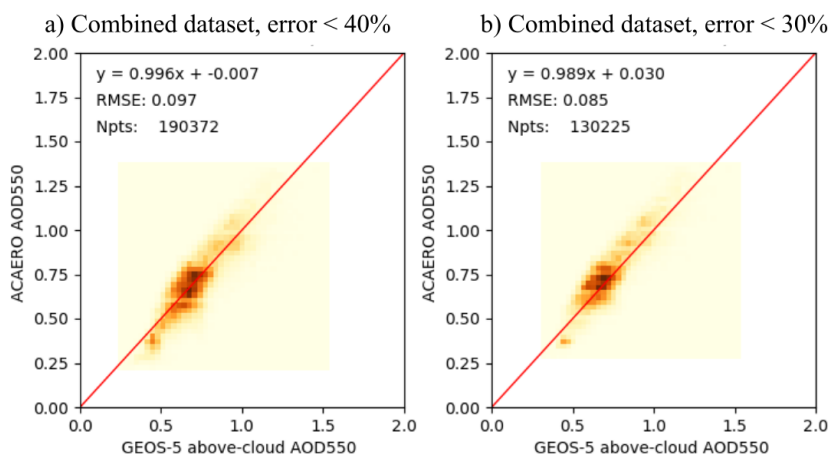
653 Figure 8. MOD06ACAERO retrieval results from the combined dataset of Figure 3a  
654 compared to source GEOS-5 aerosol optical depth. AOD retrievals where COT was less than  
655 and where the scattering angle was in the cloud bow are now discarded. Additionally the  
656 data extent had been limited to only include pixels with view zenith angle of less than 32  
657 degrees. Retrieval comparison shows further improvement. Panel a) shows MOD06ACAERO  
658 retrievals with uncertainty of less than 40% and panel b) shows same with uncertainty less  
659 than 30%.





660 Figure 9. MOD06ACAERO retrieval results from the combined dataset of Figure 3a  
661 compared to source GEOS-5 aerosol optical depth. AOD retrievals where COT was less than  
662 24 and where the scattering angle was in the cloud bow are now discarded. Additionally the  
663 data extent had been limited to only include pixels with view zenith angle of less than 20  
664 degrees. Retrieval comparison shows further improvement however it is not clear if the  
665 reduction in dataset size is worth the gain in accuracy. Panel a) shows MOD06ACAERO  
666 retrievals with uncertainty of less than 40% and panel b) shows same with uncertainty less  
667 than 30%.

668  
669



670 Figure 10. MOD06ACAERO retrieval results from simulated MCARS granule based on Terra  
671 MODIS 2006 day 224 10:05 UTC compared to source GEOS-5 aerosol optical depth. In this  
672 experiment both MOD06 and MOD06ACAERO were modified to use MCARS pixel-level  
673 atmospheric profiles to perform atmospheric correction. AOD retrievals where COT was less  
674 than 4 and where the scattering angle was in the cloud bow are now discarded. Additionally  
675 the data extent had been limited to only include pixels with view zenith angle of less than 20  
676 degrees. This experiment shows excellent agreement with source data. Panel a) shows  
677 MOD06ACAERO retrievals with uncertainty of less than 40% and panel b) shows same with  
678 uncertainty less than 30%. The small dataset size in panel b) is the reason for slightly lower  
679 agreement with source compared to panel a)  
680